J. Fluid Mech. (1987), *vol.* 183, *pp.* 399–420
Printed in Great Britain

Cellular flows of a viscous liquid that partly fills a horizontal rotating cylinder

By T. BROOKE BENJAMIN
Mathematical Institute, 24/29 St Giles, Oxford OX1 3LB, UK

AND S. K. PATHAK
Department of Civil Engineering, University of Roorkee, Roorkee U.P., India

(Received 5 December 1986)

This theoretical and experimental investigation inquires into the various steady and unsteady motions that are possible when a highly viscous liquid partly fills a closed circular cylinder rotated about its horizontal axis at constant angular velocity. Fillings leaving an air bubble in the range roughly 10–20% by volume provide the most lively variety of observable phenomena.

The full hydrodynamic problem is too complicated to be amenable to quantitative theoretical treatment, except by numerical analysis which is not yet available; but the abstract qualitative theory developed in §2 appears to capture all the essentials of experimentally found behaviour. An analogous finite-dimensional system, such as would be presented by a close finite-element approximation, is used to illuminate principles governing the order of multiple solutions and their stability. Then the connection between the full problem and the analogue is demonstrated. Finally a simple argument is outlined confirming the observed stability of the motion at small rates of rotation.

The experiments are described in §3 and their results presented in §4. For various values of the cylinder's aspect ratio, estimated singularities of the time-independent solution set are recorded as several-branched graphs of $\omega\nu/gR$ versus volume fraction filled by liquid (ω is the angular velocity of the container, R its radius and ν the kinematic viscosity of the liquid). The experimental observations are discussed in §5.

1. Introduction

The class of nonlinear phenomena examined here was probably noticed many times in the distant past, but the first record of it known to us is a brief note by Balmer (1970). The most prominent effects in question are easy to demonstrate roughly and they are very striking. An accurate, repeatable account of them experimentally is quite demanding, however, which fact may explain why no thorough investigation has yet appeared.

An example of these cellular flows is shown in figure 1, although this photograph is not a view of the apparatus used in the experiments to be reported. A transparent, circular cylindrical container is filled partly (85%, say) with a highly viscous liquid and closed off, so that an air bubble is left inside. The cylinder is mounted with its axis horizontal and is rotated about the axis at constant angular velocity ω. When ω is small enough, the bubble assumes an elongated stationary form near the top of the cylindrical space, being covered above by a thin layer of moving liquid but otherwise not being much different from its configuration when the cylinder is at rest.

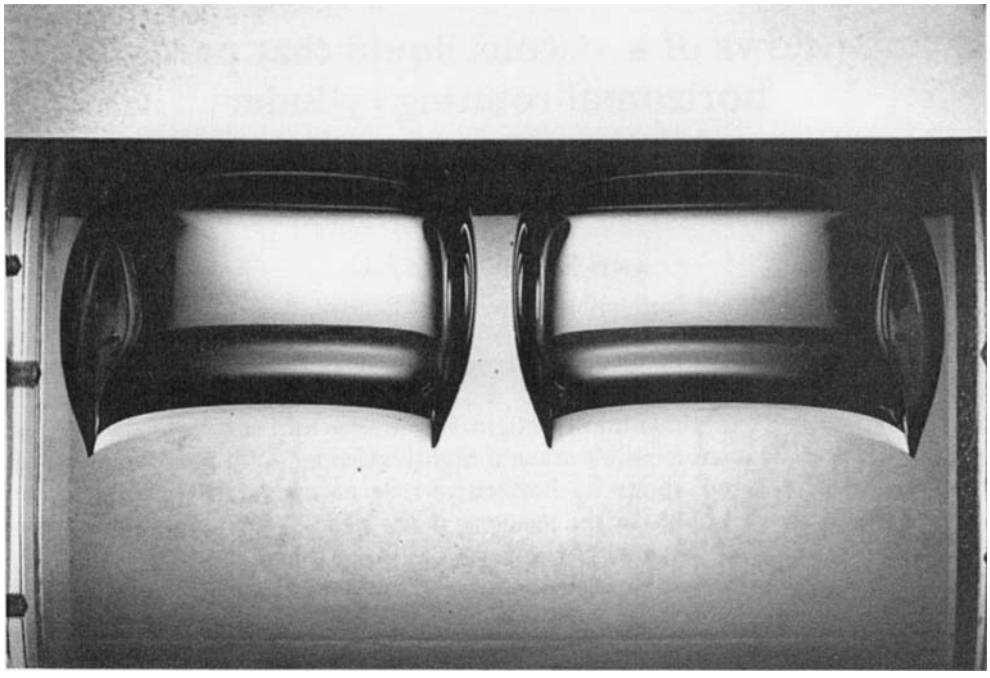

FIGURE 1. Example of steady form taken by bubble after division into two parts, viewed in horizontal direction perpendicular to axis of rotating cylindrical container.

As ω is gradually increased from small values, the bubble is displaced progressively further in the direction of rotation; and ultimately, when ω is raised to a critical value ω_c, the bubble suddenly divides and evolves into a stationary form in two disjoint parts as shown in figure 1. (The transformation into just two bubbles depends, of course, on the aspect ratio of the cylinder being not too great; in our experiments the length was at most 3.4 times the radius.) With the bubble in its divided state, gradual reductions in ω can be made to well below ω_c before finally there is an abrupt reversion to the undivided form. Thus a strong hysteresis is demonstrable. This and several other nonlinear effects, involving both stationary and time-dependent motions, are to be examined in detail.

We confine attention to the case where the viscosity of the liquid is high enough for inertial effect to be negligible. Evidently an interesting range of phenomena is compatible with this simplification, which makes a theoretical account accessible although still quite difficult. For his experimental observations Balmer (1970) used heavy oils, but their viscosities were probably not high enough to make the present model secure; so the phenomena in question should not be considered tied exclusively to situations where a Stokes-flow approximation is accurate. On the other hand, our experiments using Golden Syrup were designed to obviate the further complications of significant inertial effects.

Cellular structures exhibited by internal free surfaces in rapidly rotating liquids of *small* viscosity have been reported by various authors (e.g. Phillips 1960; Debler & Yih 1962; Karweit & Corrsin 1975); and no doubt the same general principles from singularity theory as will be used interpretively here could be applied also to some of these other observations. But nothing in this direction will be attempted at present.

Other notable antecedents are the theoretical papers by Ruschak & Scriven (1976) and Orr & Scriven (1978) dealing with steady 'rimming flow' of a liquid with free surface inside a horizontal rotating cylinder. The latter paper has particular interest in presenting exemplary numerical solutions of the full Navier–Stokes equations with free-boundary conditions accounting for gravity and surface tension. But the theoretical model is two-dimensional, so having little relevance to the present topic.

We must acknowledge, however, that our work has considerable affinity with the investigation by Moffatt (1977), which dealt with waveforms in the free surface of a viscous film transported on the outside of a rotating solid cylinder, and also the recent investigation by Pritchard (1986) into the multiplicity of states observable when a viscous liquid flows over the end of a broad inclined plate. To explain his practical observations, Moffatt developed a largely satisfactory account based on approximations akin to those of lubrication theory; but this approach seems unavailing for the present problem. Contrarily, it may be appreciated that for Moffatt's problem *in toto*, for Pritchard's and indeed for any other problem of highly viscous flow with a free surface under gravity and surface tension, the general theoretical frame to be assembled below is almost immediately serviceable and its qualitative conclusions can guide the interpretation of observed phenomena.

The theory presented in §2 has two stages. First, in §2.1, the properties of a finite-dimensional nonlinear evolutionary system analogous to the hydrodynamic system are examined in sufficient detail to establish general principles bearing on the classification of multiple steady solutions, their possible patterns of behaviour as parameters are varied and their stability. Then, in §2.2, the precise relation between the hydrodynamic system and the analogue is exposed, revealing a powerful source of qualitative information. The complete problem appears to be far too difficult for quantitative theoretical predictions with any reliability, except by numerical means which would still be difficult and nobody has yet tried. Thus the oblique, abstract approach adopted is enforced by necessity, and short of still needed mathematical precision as regards function classes and the better definition of formal operations it goes about as far as seems feasible at present. Perhaps the most persuasive justification for the two-stage description is that, when numerical solutions by finite elements are attempted in due course, the model examined in §2.1 should be exemplified essentially.

The experiments reported in §§3 and 4 cover an admittedly narrow parameter range but do so more or less comprehensively. Their aim was to establish in the light of the theory a secure demonstration of principles underlying observable behaviour, and we eschewed the huge variety of striking flow patterns – comparable with the variety in Pritchard's interesting study – that is possible in rotating, partly filled cylinders of greater length.

2. Theory

The flow system in question is too complicated to be amenable to constructive treatment, except perhaps by numerical analysis which may in due course be attempted. Here only a number of qualitative facts about it will be established, but they appear to capture its salient mathematical properties.

2.1. *Finite-dimensional analogue*

For reasons to be explained presently, a close affinity can be appreciated to exist between this flow system and the finite-dimensional system described as follows,

which too is controlled by dissipative effects and is free from inertial effects. Suppose the configuration of the model system to be determined by generalized coordinates $q_k\,(k = 1, 2, \ldots, n)$, denoted collectively by $\boldsymbol{q}$, and write $\dot{q}_k = \mathrm{d}q_k/\mathrm{d}t$, collectively $\dot{\boldsymbol{q}} = \mathrm{d}\boldsymbol{q}/\mathrm{d}t$. In general any motion of the system is described by the n ordinary differential equations

$$\frac{\partial F}{\partial \dot{q}_k} + \frac{\partial V}{\partial q_k} = 0, \tag{1}$$

in which $F: \mathbb{R}^{2n} \to \mathbb{R}$ is a Rayleigh dissipation function depending on $\boldsymbol{q}$ and $\dot{\boldsymbol{q}}$ (cf. Lamb 1932, §368) and $V: \mathbb{R}^n \to \mathbb{R}$ depending only on $\boldsymbol{q}$ is the potential energy of the system. In common with the simplest examples of systems with dynamical equations in the form (1), F is a quadratic function of $\dot{\boldsymbol{q}}$; but a crucial difference here is that F is not homogeneous in $\dot{\boldsymbol{q}}$. Specifically, using the convention that summation over $1, \ldots, n$ is implied by each repeated subscript, we suppose that

$$F = \tfrac{1}{2} a_{kl}(\boldsymbol{q})\,[\dot{q}_k + Q_k(\boldsymbol{q})]\,[\dot{q}_l + Q_l(\boldsymbol{q})], \tag{2}$$

where (a_{kl}) is a given *symmetric* matrix of functions of $\boldsymbol{q}$ alone which is positive definite for all $\boldsymbol{q}$, and the Q_i are given functions of $\boldsymbol{q}$ alone depending on a parameter, say ζ. Thus the equations (1) become

$$a_{kl}\,\dot{q}_l + \frac{\partial V}{\partial q_k} + R_k = 0 \tag{3}$$

with $R_k = a_{kl}\,Q_l$ evaluated in $\boldsymbol{q}$.

A steady state of the system (3) is a solution, say $\overline{\boldsymbol{q}}$, of the equations

$$f_k(\overline{\boldsymbol{q}}) \equiv \left(\frac{\partial V}{\partial q_k} + R_k\right)(\overline{\boldsymbol{q}}) = 0; \tag{4}$$

and plainly its stability depends on the roots λ of the determinantal equation

$$\det\,[\lambda a_{kl}(\overline{\boldsymbol{q}}) + M_{kl}(\overline{\boldsymbol{q}})] = 0, \tag{5}$$

where

$$M_{kl} = \frac{\partial f_k}{\partial q_l} = \frac{\partial^2 V}{\partial q_k\,\partial q_l} + \frac{\partial R_k}{\partial q_l}.$$

Excluding for the moment the case of a zero or purely imaginary root, we recognize that the state $\overline{\boldsymbol{q}}$ is stable if and only if all the roots λ have negative real parts. Note that the matrix (M_{kl}) is generally not symmetric because $(\partial R_k/\partial q_l)$ is not, so the symmetry and positive definiteness of (a_{kl}) do not guarantee that all the roots λ are real. The possibilities of spiralling orbits close to $\overline{\boldsymbol{q}}$ and of Hopf bifurcations are thus admitted by the present system.

Let us next consider how to classify multiple solutions of (4), which may interact at singular points as the functions Q_i and hence R_i are varied parametrically. For the reason mentioned just above, more specifically because $\epsilon^{klm}\,\partial R_l/\partial q_m \neq 0$ in general, the n-vector $\boldsymbol{R}$ cannot be represented as the gradient of a scalar. Consequently, elementary Morse theory cannot be used for the present purpose. Brouwer degree theory is applicable, however, and it accounts neatly for the main properties in view (cf. Lloyd 1978, Chapters 1 and 2).

Let us suppose for the sake of clarity that $V \in C^2(\mathbb{R}^n \to \mathbb{R})$ and $\boldsymbol{R} \in C^1(\mathbb{R}^n \to \mathbb{R}^n)$, so that each component of (M_{kl}) is a continuous function; but it would in fact suffice that

$\boldsymbol{f}$ is continuous $\mathbb{R}^n \to \mathbb{R}^n$ (Lloyd, §1.4). Again momentarily excepting the singular case where $\det[M_{kl}(\overline{\boldsymbol{q}})] = 0$, we define the *index* of a solution $\overline{\boldsymbol{q}}$ of (4) to be

$$i(\overline{\boldsymbol{q}}) = \pm 1 \quad \text{accordingly as} \quad \det[M_{kl}(\overline{\boldsymbol{q}})] \gtrless 1. \tag{6}$$

Note that the determinant in (6) equals the product of all eigenvalues of $(M_{kl}(\overline{\boldsymbol{q}}))$; so $i(\overline{\boldsymbol{q}})$ defined by (6) is the same as $(-1)^\beta$, where β is the number of negative real eigenvalues with allowance for multiplicity. Complex eigenvalues occur in conjugate pairs and so do not affect the expression for $i(\overline{\boldsymbol{q}})$.

Next, with reference to any bounded domain $\Delta \subset \mathbb{R}^n$ with no solution of (4) on its boundary $\partial\Delta$ but with $N \geqslant 0$ solutions $\overline{\boldsymbol{q}}^{(1)}, \ldots, \overline{\boldsymbol{q}}^{(N)}$ in its interior, the *degree* of $\boldsymbol{f}$ relative to Δ is defined as the integer

$$\left.\begin{aligned} \deg(\boldsymbol{f}, \Delta) = \sum_{m=1}^{N} i(\overline{\boldsymbol{q}}^{(m)}) \qquad & \text{if } N \geqslant 1, \\ = 0 \qquad & \text{if } N = 0. \end{aligned}\right\} \tag{7}$$

Degree is otherwise calculable from the action of $\boldsymbol{f}$ on $\partial\Delta$ alone, and the definition is thus extensible to cover the critical case of solutions with $\det[M_{kl}] = 0$. The index of such solutions is generally 0 or ± 1, but rarely may be any integer, according to how the critical point in Δ is unfolded as a parameter of $\boldsymbol{f}$ is varied. The most useful properties of degree in present respects are listed as follows.

(i) Suppose that, as a parameter ζ of $\boldsymbol{f}$ is varied continuously over a closed interval $\mathscr{I}$, no solution of (4) occurs on the boundary $\partial\Delta$ of Δ. Then $\deg(\boldsymbol{f}, \Delta)$ remains the same for all $\zeta \in \mathscr{I}$.

This property ensures that, as ζ or any other parameter is varied continuously, changes in the solution set can occur only in strictly limited patterns. For example, new solutions cannot arise singly; nor can solutions disappear singly. As illustrated in figure 2(*a*), on the other hand, solutions can arise or disappear as a pair branching from a singular point with index 0. Away from the singular point (turning point) one branch of solutions has index 1 and the other has index -1. Two other well-known patterns of behaviour complying with property (i) are illustrated in figures 2(*b*) and 2(*c*), being explained in the caption, and together with the first case they suffice to account for the main experimental observations to be presented later.

(ii) Being in effect a special case of (i), the next property is useful for calculating $\deg(\boldsymbol{f}, \Delta)$ directly from knowledge of $\boldsymbol{f}: \partial\Delta \to \mathbb{R}^n$. Consider the homotopy $\boldsymbol{H}(s) = s\boldsymbol{f} + (1-s)\boldsymbol{I}$, $0 \leqslant s \leqslant 1$. If there is no element $\boldsymbol{q} \in \partial\Delta$ satisfying $s\boldsymbol{f}(\boldsymbol{q}) + (1-s)\boldsymbol{q} = 0$ for any $s \in [0, 1]$, then $\deg(\boldsymbol{H}(s), \Delta)$ is independent of s in this interval. Thus $\deg(\boldsymbol{f}, \Delta) = \deg(\boldsymbol{I}, \Delta)$, which is 1 if $\boldsymbol{0} \in \Delta$.

To incorporate an attribute typical of hydrodynamic problems, it may be supposed that the condition for this property to hold is satisfied when Δ is a ball $|\boldsymbol{q}| < r$ of sufficiently large radius r. Then the sum of the indices of all time-independent solutions is 1. Consequently, except at critical parameter values, the number N of such solutions is odd, being composed of $\frac{1}{2}(N+1)$ solutions with index 1 and $\frac{1}{2}(N-1)$ with index -1. Although not yet proven, this situation appears to apply in the flow system examined below.

(iii) Any non-critical solution $\overline{\boldsymbol{q}}$ of (4) with $i(\overline{\boldsymbol{q}}) = -1$ is an unstable solution of (3). To prove this property consider the determinant on the left of (5) as a function of real $\lambda \geqslant 0$. By the definition (6) of index, the determinant is negative for $\lambda = 0$ in the present case. But it must become positive for sufficiently large λ because $\det(a_{kl})$ is

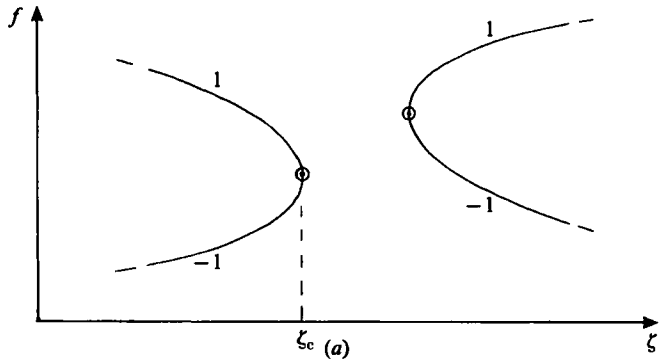

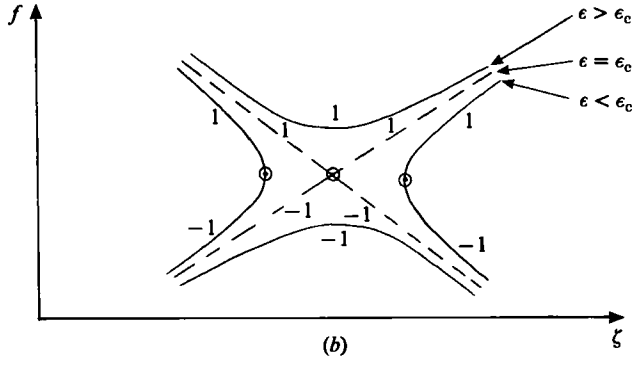

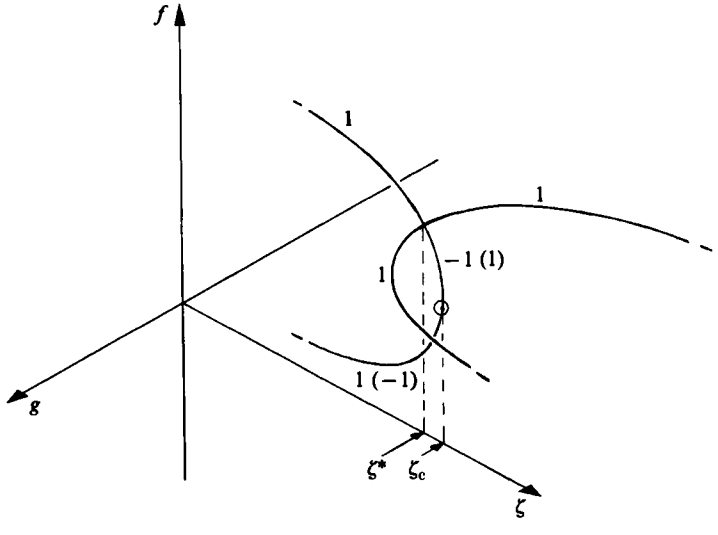

(c)

FIGURE 2. Examples of singularities in solution set parameterized by ζ. Here f is any function discriminating between solution branches; and singular points with index 0 are circled. (*a*) Branches with indices **1** and **−1** terminated at turning point. (*b*) Unfolding of transcritical bifurcation as second parameter ϵ is varied. (*c*) Symmetry-breaking bifurcation from stable branch in (ζ, f)-plane, asymmetric part of solution being represented by $\pm g$. Indices calculated only in the class of symmetric functions are given in parentheses (cf. §5).

positive as a necessary condition for the poitive-definiteness of (a_{kl}). Therefore (5) has a real root $\lambda_1 > 0$, and an implication of (5) is that there is a non-zero vector $\boldsymbol{\eta} \in \mathbb{R}^n$ satisfying

$$\lambda_1 a_{kl}\eta_l + M_{kl}\eta_l = 0 \qquad (k = 1, \ldots, n).$$

The equations linearizing (3) relative to $\bar{\boldsymbol{q}}$ thus have a solution $\boldsymbol{\eta}\exp(\lambda_1 t)$ which increases without bound as $t \to \infty$. Consequently, since the terms ∇V and $\boldsymbol{R}$ in (3) are continuous in $\boldsymbol{q}$ the Lyapunov stability of $\bar{\boldsymbol{q}}$ is denied in respect of every relevant metric.

Because of (iii) the condition $i = 1$ is necessary for stability of a non-critical stationary solution. But it is not a sufficient condition for stability. (For example, both M and $a^{-1}M$ may have just two negative real eigenvalues, so that the respective steady solution $\bar{\boldsymbol{q}}$ has $i = 1$ but is evidently unstable.)

It is noteworthy that the same set of general rules referred to Leray–Schauder degree was shown by Benjamin (1976) to apply to steady solutions of the Navier–Stokes equations in bounded domains with solid, tangentially moving boundaries. The simple proof of (iii) above compares with the proof of Theorem 3 in the cited paper. In various subsequent papers (e.g. Benjamin 1978*a*, *b*; Benjamin & Mullin 1982; Cliffe & Mullin 1985) these rules have been used extensively to explain observed bifurcation phenomena in fluid flows at moderate Reynolds numbers.

2.2. *The hydrodynamic problem*

Returning to the problem described in §1, we have to establish its relation with the simpler system discussed above. Let D_0 denote the domain occupied by the bubble, which domain generally depends on time t and is not necessarily connected or simply connected, and let S denote its boundary, the free surface. The domain occupied by the viscous liquid is denoted by D, so that the interior of the circular cylinder is $D_0 \cup S \cup D$, and the outer boundary composed of the solid cylindrical wall and plane endwalls is denoted by B. In terms of Cartesian coordinates the closed surface S has an arbitrary parametric description in the form

$$x_i = X_i(\alpha, \beta, t) \qquad (i = 1, 2, 3), \tag{8}$$

where (α, β) ranges over a fixed rectangle Ω; and we can particularize the description to the extent that the functions X_i become independent of t when the bubble is steady (i.e. (8) is not a Lagrangian description of the motion of liquid particles in S). The functions X_i are considered to constitute the solution of the problem, fully describing the observable shape, size, and position of the bubble. For similar uses of a parametric representation in treatments of free-surface problems, reference may be made to two recent papers (Benjamin & Olver 1982, Appendix 1; Benjamin 1987, §2).

Considering $\gamma_1 = \partial(X_2, X_3)/\partial(\alpha, \beta)$ together with γ_2 and γ_3 correspondingly defined in cyclic order, and writing $J = (\gamma_i^2)^{\frac{1}{2}} \geqslant 0$ (with summation convention), we note γ_i/J to be the components of the unit normal $\boldsymbol{n}$ to S directed into the liquid. The area of S is

$$|S| = \int_S \mathrm{d}s = \int_\Omega J \,\mathrm{d}\alpha\,\mathrm{d}\beta;$$

and we shall use the well-known fact that the first variation of $|S|$ is given by

$$\delta|S| = \int_\Omega 2H\gamma_i \,\delta X_i \,\mathrm{d}\alpha\,\mathrm{d}\beta, \tag{9}$$

where H is the (inward) mean curvature of S. (The notation of (9) and comparable expressions to follow should be understood to abbreviate the formal definition of a Gateaux derivative with respect to the inner product for $L^2(\Omega)$ (cf. Benjamin 1987, §2).)

The volume of the bubble is assumed to be fixed. Therefore its potential energy is

$$V = \sigma|S| + \int_{D_0} \rho g x_3 \, dx_1 \, dx_2 \, dx_3, \tag{10}$$

where σ is the coefficient of surface tension, ρ is the density of the liquid and x_3 is a coordinate directed vertically downward. Hence, according to a standard definition and in view of (9), the functional derivatives of V with respect to variations in X_i, subject to the constraint that the volume of D_0 is fixed, are seen to be

$$\frac{\delta V}{\delta X_i} = (2\sigma H + \rho g X_3 - P)\,\gamma_i \qquad (i = 1, 2, 3). \tag{11}$$

The Lagrange multiplier P respecting the volume constraint can be identified with the constant pressure inside the bubble.

To describe the motion of the liquid, consider the velocity $\boldsymbol{u} = (u_1, u_2, u_3)\,(\boldsymbol{x}, t)$ and pressure $p(\boldsymbol{x}, t)$ defined over D. It is convenient to express the stress tensor relative to hydrostatic pressure, thus

$$\tau_{ij} = -(p - \rho g x_3)\,\delta_{ij} + 2\mu e_{ij}(\boldsymbol{u}), \tag{12}$$

where μ is the viscosity of the liquid and

$$e_{ij}(\boldsymbol{u}) = \tfrac{1}{2}(u_{i,j} + u_{j,i})$$

is the strain-rate tensor. The assumed incompressibility of the liquid requires

$$\operatorname{div} \boldsymbol{u} = u_{i,i} = 0 \qquad \text{in } D; \tag{13}$$

and on the assumption that inertial effects are negligible the dynamical equations are

$$\tau_{ij,j}(\boldsymbol{u}) = 0 \qquad \text{in } D. \tag{14}$$

The cylindrical container rotates about its axis with singular velocity ω, and it will be helpful to introduce the notation $\omega \boldsymbol{U}\,(\equiv \boldsymbol{\omega} \times \boldsymbol{x}$ in the obvious sense) for the velocity field corresponding to rigid rotation everywhere with this angular velocity. The boundary conditions at the solid walls of the container are then expressible by

$$\boldsymbol{u} = \omega \boldsymbol{U} \qquad \text{on } B, \tag{15}$$

and it is of course through (15) that the parameter ω enters the mathematical problem. The boundary conditions at the free surface S are next considered. First, there is the kinematic condition relating the normal component of velocity in the liquid and the rate at which S is displaced normally; thus we have

$$\gamma_i u_i = \gamma_i \dot{X}_i \qquad \text{on } \Omega \tag{16}$$

with $\dot{X}_i = \partial X_i / \partial t$. (Note the deliberate use of γ_i in (16), rather than equivalently $n_i = \gamma_i / J$, and reference to Ω rather than S. This distinction highlights that $\boldsymbol{u}|_S$ will like $\boldsymbol{X}$ be considered abstractly as a function of α, β and t.) Secondly, there is the condition of zero tangential stress, which is expressible for $i = 1, 2, 3$ by

$$\gamma_j \tau_{ij} - \gamma_i n_j n_k \tau_{jk} = 0 \qquad \text{on } \Omega. \tag{17}$$

The third and final condition at the free surface represents the balance of normal stress in the liquid against the net effect of the pressure inside the bubble and the normal-stress discontinuity due to surface tension. Thus, using (17) and recalling the special definition (12) of τ_{ij}, we have

$$\gamma_i(n_j n_k \tau_{jk}) = \gamma_i(-P+2\sigma H+\rho g X_3) \qquad \text{on } \Omega. \tag{18}$$

Now, it is known that, for a given instantaneous configuration of the free boundary S, the velocity $\boldsymbol{u}$ in D is uniquely determined as a solution of (13), (14) and just the three boundary conditions (15), (16) and (17). In fact, according to the variational principle discovered by Korteweg (1883), as elaborated comprehensively by Keller, Rubenfeld & Molyneux (1967, §2) and extended by Skalak (1970) to include the effects of surface tension, the solution $\boldsymbol{u}$ can be characterized uniquely as follows. Among all solenoidal vector fields defined in D and satisfying these boundary conditions, $\boldsymbol{u}$ is the minimizer of the convex functional $\mathscr{D}-2\dot{V}$, where $\mathscr{D}$ expresses the rate of dissipation in the liquid and $\dot{V} = \mathrm{d}V/\mathrm{d}t$. Since $\boldsymbol{u}$ is thus uniquely determined as a transformation of $\boldsymbol{X}$ and $\dot{\boldsymbol{X}}$, its dependence on the parameter ω being imposed by (15), the remaining boundary condition (18) constitutes the functional relation between $\boldsymbol{X}$ and $\dot{\boldsymbol{X}}$ that decides the evolution of S.

To expose the essential form of this relation, details of the Korteweg principle are now presented in a new light (cf. Keller *et al.* 1967, §2). The dissipation function akin to that introduced in (1) is $F = \frac{1}{2}\mathscr{D}$, so being the integral of the scalar $\frac{1}{2}\tau_{ij}(\boldsymbol{u})\, e_{ij}(\boldsymbol{u})$ over D. Because of (12) which implies $e_{ii} = 0$, we thus have

$$F = \int_D \mu[e_{ij}(\boldsymbol{u})]^2 \,\mathrm{d}v, \tag{19}$$

where $\mathrm{d}v$ is short for $\mathrm{d}x_1\,\mathrm{d}x_2\,\mathrm{d}x_3$. The next step is to consider the variation of F due to infinitesimal variations of $\dot{\boldsymbol{X}}$ with $\boldsymbol{X}$ held fixed, so that S and D are not varied. Evidently this is

$$\delta F = \int_D 2\mu\, e_{ij}(\boldsymbol{u})\, e_{ij}(\delta\boldsymbol{u})\,\mathrm{d}v; \tag{20}$$

and because of (13) the integrand is the same as

$$\begin{aligned} \tfrac{1}{2}\tau_{ij}(\boldsymbol{u})\,(\delta u_{i,j}+\delta u_{j,i}) &= \tau_{ij}(\boldsymbol{u})\,\delta u_{i,j} \\ &= [\tau_{ij}(\boldsymbol{u})\,\delta u_i]_{,j} - \tau_{ij,j}(\boldsymbol{u})\,\delta u_i \\ &= [\tau_{ij}(\boldsymbol{u})\,\delta u_i]_{,j}, \end{aligned}$$

where the first equality follows from the symmetry of τ_{ij} and the last from (14). Since the integrand is thus a divergence, the integral expressing δF can be reduced by Gauss's theorem to a surface integral over the boundary $S \cup B$ of D. The integral over B is zero because $\delta\boldsymbol{u} = 0$ there, and so the result is

$$\begin{aligned} \delta F &= -\int_S n_j\,\tau_{ij}(\boldsymbol{u})\,\delta u_i \,\mathrm{d}s \\ &= -\int_\Omega \gamma_j\,\tau_{ij}(\boldsymbol{u})\,\delta u_i \,\mathrm{d}\alpha\,\mathrm{d}\beta. \end{aligned} \tag{21}$$

(Remember that $\boldsymbol{n}$ is directed into D.)

With S fixed, (16) implies that

$$\gamma_i\,\delta u_i = \gamma_i\,\delta\dot{X}_i. \tag{22}$$

Moreover, this basic relation between $\delta \boldsymbol{u}$ and $\delta \dot{\boldsymbol{X}}$ can be used to reduce (21) when the tangential-stress condition (17) satisfied by $\boldsymbol{u}$ is used. Thus we deduce finally that

$$\delta F = -\int_{\Omega} [n_j n_k \tau_{jk}(\boldsymbol{u})] \gamma_i \, \delta \dot{X}_i \, \mathrm{d}\alpha \, \mathrm{d}\beta. \tag{23}$$

This identity holds for arbitrary $\delta \dot{\boldsymbol{X}}$ subject only to the constraint

$$\int_{\Omega} \gamma_i \dot{X}_i \, \mathrm{d}\alpha \, \mathrm{d}\beta = 0 \tag{24}$$

imposed by incompressibility of the liquid. Thus (23) establishes that

$$\frac{\delta F}{\delta \dot{X}_i} = -[n_j n_k \tau_{jk}(\boldsymbol{u})] \gamma_i, \tag{25}$$

where terms (const.)γ_i respecting the constraint (24) can be left implicit on the right-hand side since they will be subsumed by the terms $-P\gamma_i$ in (11). (In other words, the concomitant constraints that the liquid is incompressible and that the volume of D_0 is fixed will be represented in (26) below by the single Lagrange multiplier P.)

Comparing (18) with (11) and (25), we see that the evolutionary system of equations for the bubble surface S is expressible as

$$\frac{\delta F}{\delta \dot{X}_i} + \frac{\delta V}{\delta X_i} = 0 \qquad (i = 1, 2, 3), \tag{26}$$

which compares with (1). This conclusion is admittedly formal, but it appears to be the key to understanding the complicated behaviour observed experimentally.

Much nevertheless remains to be done towards clarifying the mathematical problem, which is far from easy. In particular, there is a need to clarify the transformations implicit in (26) by identifying them as operations on appropriate function classes for $\boldsymbol{X}$ and $\dot{\boldsymbol{X}}$. A more demanding objective is to confirm that a degree theory akin to the one outlined in §2.1 applies to the set of steady solutions, for which of course the terms $\delta F/\delta \dot{X}_i$ in (26) do not vanish unless $\omega = 0$. A difficulty facing any attempt to formulate such a theory is spotlighted by the experimental facts: namely, for certain steady solutions D_0 is divided, so that the bubble surface S bounding D_0 has disjoint components. In general, therefore, representation of every steady solution $\overline{\boldsymbol{X}}$ as a continuous function of (α, β) on Ω is impossible, and continuous dependence on a third parameter unfolding discontinuities may need to be introduced for a degree-theoretic ordering of all the steady solutions. (Note that this difficulty is peculiar to a collective account of the steady solutions, not to time-dependent ones. Over an appropriate time interval T, the evolution of a divided bubble from a connected one or *vice versa* is representable as a continuous function $\boldsymbol{X}(\alpha, \beta, t)$ on $\Omega \times T$. The third parameter likely to be needed for a unified classification of steady solutions might represent the partition of the volume of D_0 between disjoint bubbles.)

Notwithstanding the incompleteness of the theory in detail, plausible implications can be drawn from (26) in the light of the comparatively simple facts established about the analogue (1). Perhaps the most telling implication is that a good finite-dimensional approximation of the hydrodynamic problem, such as by finite elements, should admit organization to present exactly the situation reviewed in §2.1.

While deferring details of a finite-element approximation as topic for subsequent

study, we may note the structural affinity between the function $\boldsymbol{X}$ of α, β, t and the approximating n-vector $\boldsymbol{q}$ introduced in §2.1, likewise between $\dot{\boldsymbol{X}}$ and $\dot{\boldsymbol{q}}$. The scalar F defined by (19) evidently is positive-definite; through (16) its dependence on $\dot{\boldsymbol{X}}$ is quadratic although not homogeneously so; and F depends in complicated fashion on $\boldsymbol{X}$ through (16) and (17). Note also that the present counterparts of $\boldsymbol{Q}$ in (2) are the time-independent velocity fields, say $\overline{\boldsymbol{u}}(\boldsymbol{x})$, that correspond to steady solutions $\overline{\boldsymbol{X}}(\alpha, \beta)$ of (26). Thus each $\overline{\boldsymbol{u}}$ is a solution of (13)–(17), with $\dot{\boldsymbol{X}} \equiv 0$ in (16), such that the respective form of S allows (18) also to be satisfied. The trivial solution $\overline{\boldsymbol{u}} = \omega \boldsymbol{U}$ in D holds uniquely in the absence of a bubble; and although *not* comparable with $\boldsymbol{Q}$ in (2) it may be considered in the following way, which illuminates the dependence of $\boldsymbol{X}(\alpha, \beta, t)$ on ω. Writing $\boldsymbol{u} = \omega \boldsymbol{U} + \boldsymbol{u}'$, we have that $\boldsymbol{u}'$ vanishes on B, satisfies (13) and satisfies (14) since $\tau_{ij}(\omega \boldsymbol{U}) = 0$. For the same reason the stress conditions (17) and (18) at the free surface have to be satisfied by $\boldsymbol{u}'$ alone; but (16) becomes

$$\gamma_i u_i' = \gamma_i (\dot{X}_i - \omega U_i) \qquad \text{on } \Omega, \tag{27}$$

which confirms as expected that the determination of $\boldsymbol{u}'$ for given S depends on $\omega \boldsymbol{U}$ as well as $\dot{\boldsymbol{X}}$. Evaluation of F and all the steps from (19) to (25), in particular (21), proceed in terms of $\boldsymbol{u}'$ exactly as in terms of $\boldsymbol{u}$. However, the facts of (26) depending implicitly on ω and its first terms not reducing simply when $\dot{\boldsymbol{X}} \equiv \boldsymbol{0}$ are perhaps made more conspicuous by (27).

Other details of the correspondence between the present system and the finite-dimensional analogue could be exhibited, but the gist of the theory is already clear enough for the interpretation of our experimental results. Two further points deserve brief attention, however, to close the theoretical discussion.

First, we should acknowledge our implicit assumption that the viscous liquid wets the solid boundary B above the top of the bubble. In other words, B and S are taken to be disjoint. This situation can be safely presumed to hold in any steady state with $\omega > 0$, and in any case when after being started from rest the cylindrical container (at which a no-slip condition always applies) has turned far enough to immerse any originally unwetted patch above the bubble. But a much more complicated situation evidently may prevail for a short time after starting, during which the present theory is inapplicable.

Finally, we outline a plausible, comparatively simple argument showing that the steady state realized at a small enough value of $\omega > 0$ is stable, as might be expected; and incidentally we demonstrate a property that corresponds to the positive-definiteness of the matrix (a_{ij}) introduced in (2). Consider the linearized perturbation equations relative to a time-dependent solution $\overline{\boldsymbol{X}}(\alpha, \beta)$ of (26). Corresponding to the perturbation

$$\boldsymbol{X} = \overline{\boldsymbol{X}} + \epsilon \boldsymbol{\xi},$$

where ϵ is infinitesimal, the velocity disturbance proportional to ϵ has two components, the first of which $\epsilon \hat{\boldsymbol{u}}$ satisfies

$$\gamma_i \hat{u}_i = \gamma_i \dot{\xi}_i \qquad \text{on } \Omega$$

and vanishes on B. Also $\hat{u}_{i,i} = 0$ and $\tau_{ij,j}(\hat{\boldsymbol{u}}) = 0$ in D. These conditions fully determine $\hat{\boldsymbol{u}}$ as a transformation of $\dot{\boldsymbol{\xi}}$ given on the free surface, and we can define an extension of $\boldsymbol{\xi}$ into D according to $\hat{\boldsymbol{u}} = \partial \boldsymbol{\xi} / \partial t$. In effect, $\epsilon \boldsymbol{\xi}$ in D is an infinitesimal change in the Lagrangian, particle description of the liquid motion, and evidently $\xi_{i,i} = 0$ in D and $\boldsymbol{\xi} = 0$ on B. The second component of the velocity disturbance is required to satisfy the tangential-stress condition (17) on the perturbed free surface, but it will not be needed explicitly.

Now, the linearization of (26) will present terms $\gamma_j \tau_{ij}(\hat{\boldsymbol{u}})$ together with terms in the other velocity component, which are comparable with the linearization of $\boldsymbol{R}$ in (3), and terms in ξ from the linearization of $\partial V/\partial X_i$. Multiplying by ξ_i, summing over i and integrating over Ω, we find the leading integral to be reducible by retracing in reverse order the steps from (20) to (21). The result to $O(\epsilon^2)$ is

$$\int_D 2\mu\epsilon^2 e_{ij}(\xi)\, e_{ij}(\xi_t)\, \mathrm{d}v = \epsilon^2 \frac{\mathrm{d}F(\xi)}{\mathrm{d}t},$$

where $F(\xi)$ is the positive-definite functional (19) evaluated in the displacement ξ rather than in velocity as before.

We hence conclude that, for an arbitrary perturbation,

$$\epsilon^2 \frac{\mathrm{d}F(\xi)}{\mathrm{d}t} = -(\text{second variation of } V \text{ evaluated in } \epsilon\xi) + (\text{quadratic term in } \epsilon\xi \text{ depending on } \omega).$$

The second term on the right will generally be comparable with that on the left, but this fact is unimportant for present purposes. If $\omega > 0$ is small enough, the bubble will be little different in form and position from the configuration that minimizes V subject to S being a complete surface (i.e. with zero contact angle between S and B). The second variation of V relative to its actual configuration will therefore still be positive, and will dominate the second term on the right provided ω is small enough. Thus we have $\mathrm{d}F(\xi)/\mathrm{d}t < 0$, whence consideration of $F(\xi) > 0$ as Lyapunov function confirms stability.

3. Experiments: apparatus and procedure

The central component of the apparatus was a high-quality cast Perspex cylinder of internal diameter 77.3 mm. One end of the cylinder was closed with a removable but tight-fitting lid made of Duralumin, into which an axle was fixed centrally. A thick Perspex lid was cemented onto the other end, and the complementary axle passing through it was tapped into a Duralumin piston which had a fairly tight sliding fit inside the cylinder. The space between the plane forward face of the piston and the plane face of the removable lid was the test section, the length L of which could be varied to any desired value. For the main sets of findings to be recorded in §4, the ratio of L to the internal radius R was adjusted to just three representative values, namely $L/R = 2.6$, 3.0 and 3.4.

The axles were mounted horizontally in bearings at each end, which together with the driving motor and gearbox described as follows were fastened to a base plate supported on levelling screws. During assembly of the apparatus before an experimental run great care was taken to check accurate alignment of the axles with the horizontal. The rotation of the cylinder was driven by a Unimatic digital stepping-motor (Model 20-2215-D) through a 6:1 reduction gearbox and flexible coupling, free of backlash, to one of the axles. The angular velocity ω of the cylinder was variable and accurately controllable over a wide range by adjustment of the pulse rate delivered to the stepping-motor unit by an electronic function-generator. A 50 MHz timer-counter was used to measure the pulse rate and hence determine ω with great accuracy.

Since the phenomena under investigation are sensitive to the viscosity of the liquid no less than to ω, comparable care was needed to control viscosity. The whole

apparatus was installed in a glass-walled box within which the temperature of circulating air was automatically maintained at 27.45 ± 0.15 °C. Experimental runs typically took many days, during all of which time the temperature of the apparatus stayed under control. The viscosity of the liquid used, Golden Syrup, was measured at the same temperature by a high-precision rheogoniometer, and its density was also measured. Most of the dimensionless results presented in §4 were calculated on the basis of the measured value of kinematic viscosity $\nu = 0.0144$ m^2 s^{-1} (i.e. 1.44×10^4 centistokes).

The volume fraction V_f of viscous liquid in the test section was a principal parameter of the experiments, being varied as follows without the need to dismantle the apparatus. Small threaded holes in the Duralumin lid were stopped off tightly by bolts when the apparatus was running; but with the apparatus at rest they could be unstopped, and through them liquid could be inserted into or withdrawn from the test section by means of a long thin metal tube connected to a syringe. After such an adjustment, V_f was estimated accurately from measurements of the bubble with a cathetometer.

For reasons to be explained in §4, it was found necessary to be able also to remove liquid from the test section while the cylinder was rotating steadily. For this purpose a modified syringe was mounted on the apparatus, rotating with the cylinder and enabling liquid to be withdrawn gradually through a coaxial hole in the axle that positioned the piston inside the cylinder.

With the test section filled to a known V_f and the whole apparatus left long enough for its temperature to have settled at the controlled level, the experimental procedure consisted for the most part in varying ω by very small steps, allowing typically at least a minute between each step, until a critical event was observed marking a loss of stability by the original state of flow. When critical values of ω, approached from above or below, had been noted roughly, the estimates of them were refined by progressively more gradual approaches to the limit of stability. Experience showed that considerable practice and care were needed to make such measurements repeatably from day to day.

4. Experimental results

Apart from the geometric ratios L/R and V_f, the parameters of the experiment are ω, the viscosity μ, density ρ and surface tension σ of the liquid, and the gravity constant g. The dimensionless number $\sigma/\rho g R^2$ indicates the relative importance of surface tension and gravity; and for our experimental conditions it is about 2×10^{-3}, small enough to indicate that surface tension was not a primary influence. Even if a lengthscale $0.1R$ is taken as more representative, the value 0.2 of this number is still small enough to support the conclusion. Although surface tension may well have been important in some of the rapid transitional events observed, also perhaps in the steady flows at the highest V_f, it seems reasonable to ignore surface tension in the scheme of dimensionless correlation for the results. Accordingly, on the supposition that the observed behaviour was essentially an interplay of viscous effects and gravity, the relevant *load parameter* is evidently the dimensionless group $\zeta = \omega\nu/gR$, where $\nu = \mu/\rho$ is the kinematic viscosity of the liquid.

Our supposition about the comparative unimportance of inertial effects, in particular centrifugal forces, is reasonably well justified. The Reynolds number $\omega R^2/\nu$ is unity for $\zeta = 0.366$, near the top of figure 3 introduced below; but for most of the phenomena recorded this Reynolds number is one or two orders of magnitude

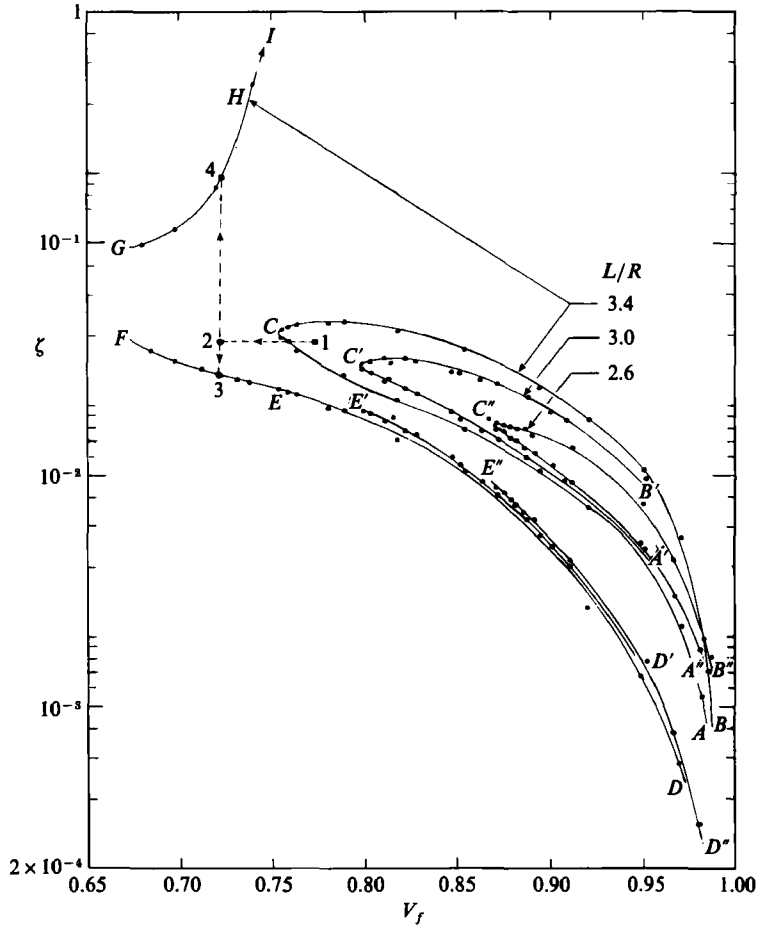

FIGURE 3. Experimentally determined critical points in (V_f, ζ)-plane, where V_f is volume fraction filled by viscous liquid and $\zeta = \omega\nu/gR$. Loci CA and CB correspond to changes from one-cell to two-cell flows, FED and GHI *vice versa*.

smaller. Although events represented in the upper part of the figure may have been affected marginally by inertia, the overall interpretation ignoring inertia appears to be secure.

Measured critical values of ζ are plotted against V_f in figure 3, and reference to the figure will help us to explain what was observed. Consider a value of V_f, say 0.85, such that a vertical line from the V_f axis interects all three of the curves ED, CA and CB respective to $L/R = 3.4$. Three critical values of ζ are thus in question, and they were estimated experimentally as follows.

First, when the apparatus had been set with $L/R = 3.4$ and $V_f = 0.85$, say, the angular velocity ω of rotation was increased in small steps from zero. At each new value of ω the air bubble contained by the moving liquid quickly underwent a minute adjustment to its elongated form near the top of the cylinder, and soon became steady again. As the first critical value ω_1 (giving $\zeta_1 = \omega_1 \nu/gR$) was approached, the upper and lower parts of the bubble surface near its middle began to dent inwards, but the form remained stable. At values of ω still nearer ω_1, time-periodic undulations appeared whose phase was observed to travel from one end of the bubble to the other.

(By reduction in size and prolongation of the steps in ω leading up to ω_1, careful attempts were made to avoid these undulations, which surprisingly broke the left–right symmetry of the original bubble relative to the central cross-sectional plane of the test space. In the end, however, it was concluded that they were an inherent feature of the motion in this narrow parameter range.) The undulations amplified when ω was raised further; and finally, at the value ω_1, the bubble began an irreversible transition, ending in the steady divided form as exemplified in figure 1. The two cells were generally more or less symmetrical relative to the central plane, but seldom exactly so. The measured ζ_1 provided one point on the curve CA in figure 3.

With the two-cell form established, ω was then reduced in small prolonged steps. The cells became progressively closer and finally, at a critical value $\omega_2 < \omega_1$, the dividing screen of liquid collapsed, whereupon the original undivided form of the bubbles was rapidly regained. The measured $\zeta_2 < \zeta_1$ provides a point on the curve ED in figure 3.

Next, from ω_2 with the single bubble well established, ω was suddenly increased to well above the first critical value ω_1. An elongated form of the bubble was thereby realized stably near the axis of the rotating cylinder, constituting a secondary mode of time-independent solutions since the morphogenesis induced by a gradual approach to ω_1 along the original solution branch had been by-passed. The value of ω was then reduced in small steps. Time-periodic undulations breaking the left–right symmetry again appeared as a critical value $\omega_3 > \omega_1$ was approached from above; and for $\omega = \omega_3$ the bubble divided just as for $\omega = \omega_1$, coming to rest in the two-cell form observed previously. The measured ζ_3 provided a point on the curve CB in figure 3.

For each volume fraction V_f the sequence of estimates $\zeta_1 \rightarrow \zeta_2 \rightarrow \zeta_3$ was repeated twice, great care being taken to approach the critical values of ω very gradually and slowly. The same measurements were made after V_f had been adjusted to each of various values; and the whole experiment was repeated with $L/R = 3.0$ and 2.6 as well as 3.4. All the experimental curves to the right of point C in figure 3 were thus gradually derived.

It is notable that the curves CA and CB respective to $L/R = 3.4$ appear to compose a cusp at their right ends, likewise $C''A''$ and $C''B''$ respective to $L/R = 2.6$. At the highest recorded values of V_f near 0.98, however, where the bubbles were quite small, control of the experiment become more difficult and the measurements were somewhat uncertain. It should be acknowledged also that measurements in the neighbourhoods of points C, C' and C'' were extremely delicate, so that estimates of curvature at these extreme points could not be made with confidence.

As will be explained in §5, the observed coincidence of the loci of ζ_1 and ζ_3 *vs.* V_f at the points C, C' and C'' implies that isolas of two-cell steady states exist for smaller values of V_f than for these points. For such values of V_f, critical values ζ_1 and ζ_3 are absent from the spectrum of single-cell states, and so there is no way to evolve the two-cell form by speed variations from the easily realizable single-cell form. To obtain measurements on the isola in the case $L/R = 3.4$, we resorted to the device describe in the penultimate paragraph of §3.

The procedure adopted can be explained by reference again to figure 3. For $L/R = 3.4$ the critical value V_{fc} of V_f, represented as the horizontal coordinate of point C, is about 0.75. With the volume fraction of liquid set to a value $V_f > V_{fc}$, ω was gradually increased from small values through ω_1, so that transition to the two-cell form occurred, and conditions were allowed to settle at a point (V_f, ζ) such as marked 1 in the figure. With the rotation rate maintained, some liquid was then

withdrawn from the test section by means of the pre-attached syringe; this process was executed very slowly to ensure that the varied conditions inside the rotating cylinder remained in the domain of attraction of the steady two-cell flow. The withdrawal of liquid was stopped at a point such as 2 in the figure, with $V_f < V_{fc}$ but with the two-cell formation still intact. From point 2, ω was very gradually reduced until at point 3 the two cells abruptly coalesced into one. The measured V_f and measured critical value ω_3 provided a point (V_f, ζ_3) on the extension EF of the previously determined curve DE. The termination at F merely represents the practical limit encountered by our technique for producing the isolated two-cell mode.

For $L/R = 3.4$ we were also able to observe the V_f-dependent upper extremity of the isola of two-cell states. Having re-established a steady two-cell state at a point such as 2, we then gradually increased ω to point 4, at which critical point the two-cells again coalesced into one. The measured critical values ζ_4 of ζ composed the curve GH in figure 3. It can be seen that GH rises very steeply at its right end; and although an extension beyond H above C certainly exists, it could not be measured with our apparatus. This limitation was considered not to be serious because along the extension of GH centrifugal effects inevitably overtake the viscous effects of primary interest here.

Experiments were tried with L/R set to values smaller than 2.6 and greater than 3.4, but additional complications were encountered indicating that the results in figure 3 adequately represent a range of distinctive, comparatively accessible phenomena. With $L/R < 2.6$ it became difficult to find critical conditions generating two-cell flows. Another phenomenon was noticed in this case when V_f was close to 1, and it was presumably much dependent on surface tension. Namely, at values of ζ somewhat higher than where splitting might have been expected, the small bubble detached from its original position of stable equilibrium and periodically circuited an orbit in the central cross-sectional plane. With $L/R > 3.4$ more than marginally, on the other hand, approaches to the critical point on the primary locus of steady single-cell states were found often to trigger morphogenesis into states with more than two cells, the final outcome being less easy to control than in the experiments described above.

5. Discussion

All the experimental observations recorded in §4 can be understood in the light of the general theory developed in §2. The theory gives no quantitative information, and indeed none is likely to be available for some time yet; but the qualitative picture provided is reasonably clear. Although a degree-theoretic ordering of the complete hydrodynamic problem has not yet been demonstrated rigorously, the direct relation shown to hold between the complete problem and its finite-dimensional analogue makes the existence of such an ordering extremely plausible. The provisional theory can therefore be addressed confidently to questions about the interrelation of multiple steady solutions and their stability.

As exposed by the experiments, the disposition of the time-dependent solution set in respect of its dependence on the load parameter ζ and secondary parameter V_f is illustrated in figure 4. This figure is schematic, referring particularly to the observations for $L/R = 3.4$, and the ordinate h could represent any property discriminating between single and divided forms of the bubble. But values 1 or 2 are assigned to h over most of the ζ-parameterized loci of stable steady states in order to highlight

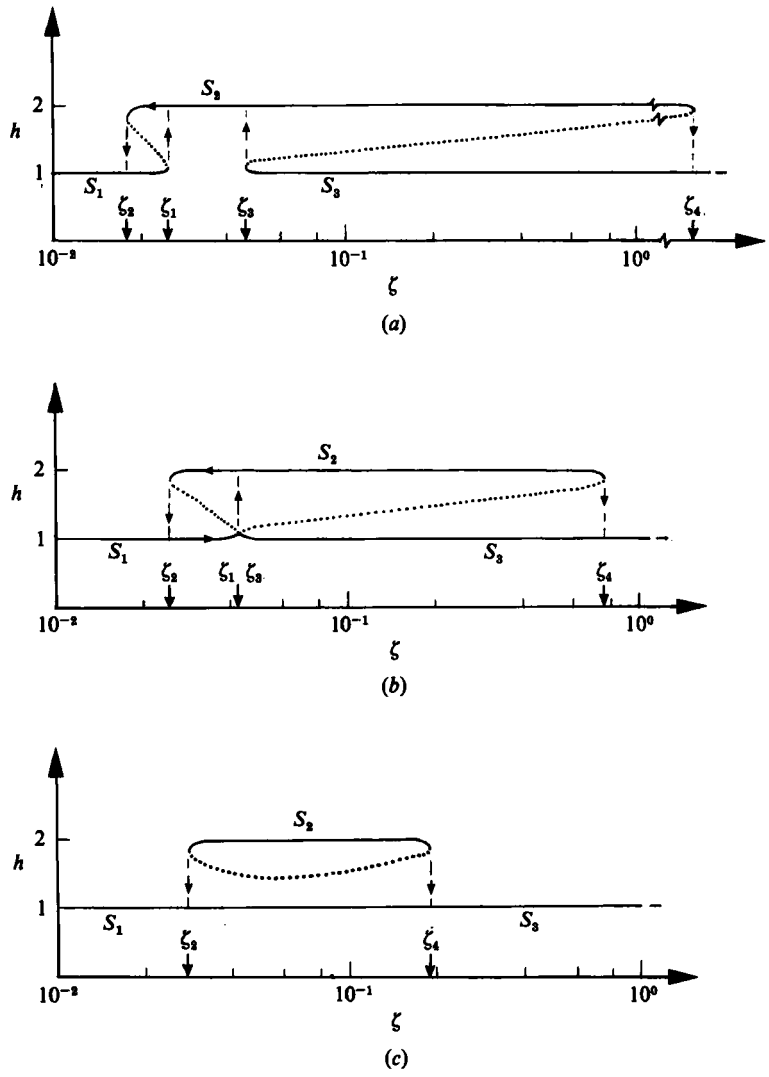

FIGURE 4. Schematic diagrams representing set of steady solutions parameterized by ζ, for several values of V_f with $L/R = 3.4$. (*a*) $V_f = 0.8\,(> V_{fc} = 0.75)$; (*b*) $V_f = 0.75 = V_{fc}$; (*c*) $V_f = 0.72\,(< V_{fc} = 0.75)$.

that flows with either one or two cells are represented. The labels S_1, S_2 and S_3 are attached respectively to the primary locus of single-cell states, which starts at small ζ and terminates at $\zeta = \zeta_1$ when $V_f > V_{fc}$, to the locus of stable two-cell states, and to the locus of single-cell states that is secondary, being disconnected from S_1, when $V_f > V_{fc}$. All three of these loci must have index $i = 1$ over most of their lengths (cf. §2.1, property (iii)), and everywhere if the possibility of symmetry-breaking bifurcations near the termini of S_1 and S_3 is excluded (see below).

Now, the theory indicates that S_1 cannot end in isolation at $\zeta = \zeta_1$. Instead it must be complemented by a branch of steady solutions with index -1, which joins S_1 at a one-sided bifurcation point (turning point) as illustrated in figure 2(*a*). Being unstable these solutions cannot be realized experimentally; but their existence must be presumed in order to make sense of the experimental observations. The unstable

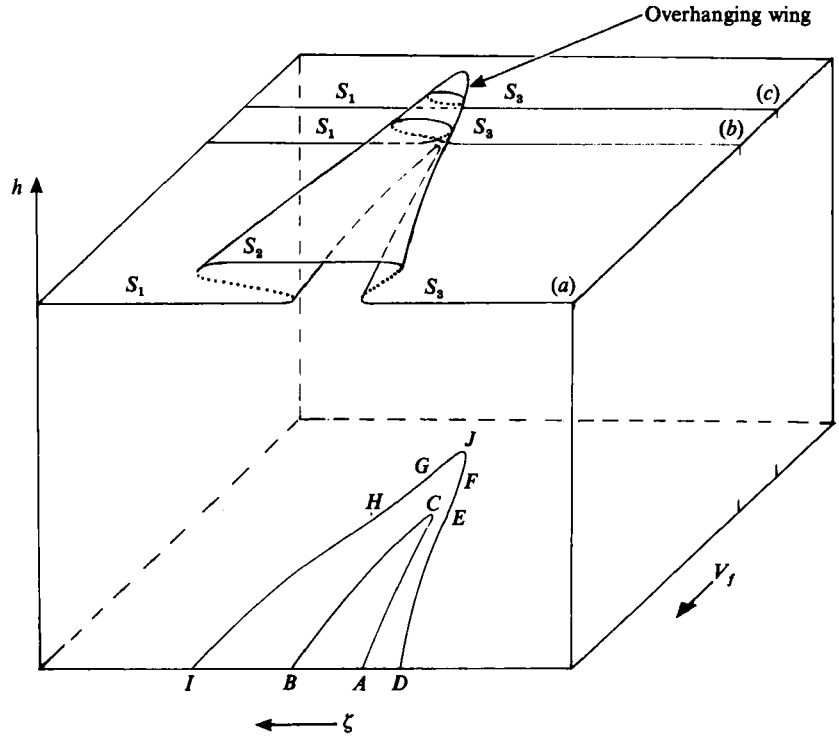

FIGURE 5. Schematic representation of solution set as folded surface above parameter plane (V_f, ζ).

branch probably joins S_2 at $\zeta = \zeta_2$, where another turning point is required to account for the observations. The observed hysteresis is indicated by arrow heads on the left in the figure. Similarly, as also illustrated in figure 4(*a*), a complementary branch of unstable solutions is implied by the observations as ζ_3 is approached from above along S_3; and it probably links with the turning point that terminates S_2 at ζ_4. This turning point at high ζ was only observed for $V_f \leqslant V_{fc}$ but presumably always exists if inertial effects are allowed; for evidently the two-cell state will always ultimately be collapsed by centrifugal force if ω is made large enough.

When the geometric parameter V_f is reduced to its critical value V_{fc} ($= 0.75$ for $L/R = 3.4$), the two turning points originally at $\zeta = \zeta_1$ and $\zeta = \zeta_3 > \zeta_1$ on S_1 and S_3 combine as a *transcritical bifurcation point*, exemplifying the process illustrated in figure 2(*b*). The four solution branches necessarily involved in the bifurcation, two with index 1 and two unstable, are unfolded for $V_f < V_{fc}$ as a continuous branch with index 1, namely the marriage of S_1 and S_3, and a continuous branch with index -1 which is therefore unstable. The locus S_2 of two-cell steady states is then wholly isolated from the primary locus, which extends continuously from $\omega = 0+$ to indefinitely high values of ω.

A three-dimensional view of this basic situation is shown in figure 5, where the arbitrary discriminating function h is plotted against position in the parameter plane (V_f, ζ). The cross-sections marked (*a*), (*b*) and (*c*) correspond, of course, to the three parts of figure 4. The extreme points C and J, corresponding to least values of V_f, are sure to be ordinary turning points, although as noted in §4 it was difficult to estimate curvature at C. The point J could not be reached experimentally, but it

presumably exists representing the final vestige of the two-cell isola. When V_f is less than its value at J, no steady two-cell state is possible.

As the results in figure 3 show, the curves of singular points in the (V_f, ζ)-plane remain basically similar when the third parameter L/R takes values smaller than 3.4. But V_{fc} becomes higher, as might be expected since the two-cell mode is obviously at a relative disadvantage in the shorter cylinder. For the same reason, the value of V_f at point J surely must increase with decreasing L/R, although we were unable to check this conclusion.

The distinctly cusp-like character of the experimental curves at their ends on the right in figure 3 is not yet understood. There is no inconsistency with the rules of singular behaviour summarized in §2.1, but we see no obvious reason for a cusp catastrophe to be exemplified – as would be presented for example, by the unfolding of figure 2 (*c*) by a symmetry-breaking parameter. A simple guess would be rather that curves such as CA and CB should terminate at a turning point, like that at C, as V_f is made close enough to 1. The possibility of surface tension becoming predominant in this region, however, coupled with that of the comparatively small bubbles being then particularly susceptible to symmetry-breaking bifurcations from a central position, make the present question an interesting target for further study.

It remains to account for the periodic undulations observed in neighbourhoods of the critical values ζ_1 and ζ_3 on the loci S_1 and S_3 when $V_f > V_{fc}$. The measurements of ζ_1 and ζ_3 were probably marginal underestimates and overestimates, respectively, because of these effects. That is, as ζ was raised towards ζ_1, the limit cycles observed to be centred on points of S_1 near its extremity will eventually have broken outside the local domain of attraction before the turning point of the steady solution set was reached. Important clues to a full explanation are given, however, by the observation that the amplitude of the undulations grew steadily from zero as ζ was increased through a narrow interval below ζ_1, suggesting a supercritical Hopf bifurcation, and above all by the observation that the unsteady motions broke the left–right symmetry of the original stable steady state.

In fact, the situation observed appears to be much the same in principle as one recently explored in great detail by Mullin, Cliffe & Pfister (1987). The comparable situation is presented over a narrow parameter range by one of the secondary modes observable in the Taylor–Couette experiment; and the cited investigation combines experimental observations and confirmatory numerical solutions of the Navier–Stokes equations by supercomputer. Of particular relevance at present, their investigation bears out predictions relating to a class of singular behaviour already much studied in modern theories of finite-dimensional dynamical systems (see Guggenheimer 1981).

The prototype in question may be summarized as follows with reference to figures 2 (*a* and *c*). Suppose that a system possessing a discrete symmetry (e.g. the left–right symmetry of our system) has a turning point in the set of time-independent *symmetric* solutions as the load parameter ζ is varied. As illustrated in figure 2 (*a*), a ζ-parameterized branch with index 1 calculated in the class of symmetric states and stable to symmetric disturbances joins at the turning point $\zeta = \zeta_c$ a branch with index -1 and so unstable in this class. It is immaterial here whether the branches exist for $\zeta > \zeta_c$ or for $\zeta < \zeta_c$; but let us fix attention on the latter case. Suppose next that at $\zeta = \zeta^* < \zeta_c$ near the turning point either the stable or unstable branch suffers a supercritical symmetry-breaking bifurcation; two branches of asymmetric steady solutions, say Γ^+ and Γ^-, being necessarily in parity and so having the same index, exists for $\zeta > \zeta^*$. This situation is illustrated in figure 2 (*c*). (It seems to be generally

true that symmetric systems are prone to symmetry-breaking bifurcations near turning points (cf. Benjamin 1978*b*, figure 6; Benjamin & Mullin 1982, §4.4).)

One may suppose also that by continuous variation of some auxiliary parameter ϵ the bifurcation point at $\zeta = \zeta^*$ can be moved into coincidence with the turning point (i.e. $\zeta^* = \zeta_c$ for $\epsilon = 0$, say). In this special case one has a bifurcation point of *codimension* 2, which description merely means that two parameters are needed for a general unfolding. This case is a rare occurrence, of course, but it is highly significant as the organizing centre for the phenomena recognizable as follows.

A reckoning of the sum of indices according to rule (i) of §2.1 establishes the following necessary facts. When indices are calculated in the class of all functions, symmetric and asymmetric, the index along one branch of symmetric solutions changes as ζ passes through $\zeta^* < \zeta_c$. Thus, if for $\epsilon > 0$ the symmetry-breaking bifurcation occurs on the symmetrically stable branch with $i = 1$ (because $\beta = 0$, where β is the number of unstable *real* eigenvalues as explained below (6)), the index of this branch becomes -1 ($\beta = 1$) in the interval (ζ^*, ζ_c), implying instability to asymmetric disturbances. Then the unstable symmetric branch has index 1 ($\beta = 2$). This disposition of indices is shown in figure 2(*c*). Again, if for $\epsilon < 0$ the bifurcation occurs on the latter branch, this branch must have $i = -1$ ($\beta = 1$) for $\zeta^* < \zeta < \zeta_c$ but $i = 1$ ($\beta = 2$) for $\zeta < \zeta^*$.

Because the branches Γ^+ and Γ^- of asymmetric solutions point in the direction of ζ increasing, opposite to that of the symmetric branches for $\zeta < \zeta_c$, their common index must accordingly be 1 in all cases. Because of their parity, moreover, Γ^+ and Γ^- cannot be detached from the loop of symmetric solutions without participation by two extra asymmetric branches with common index -1, which additional complication can be excluded typically. Therefore a continuous variation of the auxiliary parameter ϵ, through its value 0 producing the double singular point at $\zeta^* = \zeta_c$, can only move the symmetry-breaking bifurcation from one to the opposite branch of symmetric solutions. Note incidentally that the double singular point must have $i = 2$ to comply with rule (i).

The last, crucial details of this situation can now be appreciated, indicating that part of the spectrum associated with Γ^+ and Γ^- necessarily complexifies in a neighbourhood of the codimension-2 point. Note first that when bifurcating from the stable branch of symmetric solutions, Γ^+ and Γ^- must start by having $i = 1$ because $\beta = 0$; they thus exchange stability with the symmetric branch. On the other hand, when bifurcating from the unstable branch of symmetric solutions, they must start by having $i = 1$ because $\beta = 2$, thus copying properties of this branch for $\zeta < \zeta^*$. But the properties of solutions along the whole of Γ^+ and Γ^- cannot change discontinuously as ϵ passes through 0. For $\epsilon < 0$, therefore, there must be points along these branches, say $\zeta = \zeta^{**} > \zeta^*$, at which β changes from 2 to 0, specifically because the two positive (unstable) real eigenvalues in the tally $\beta = 2$ coalesce at $\zeta = \zeta^{**}$ and become a complex-conjugate pair for $\zeta > \zeta^{**}$. Just two possibilities are now in question. First, if for $\epsilon < 0$ the branches Γ^+ and Γ^- are to become stable for larger ζ, there must be points along them, say $\zeta = \zeta^{***} > \zeta^{**}$, at which with increasing ζ the complex-conjugate pair of eigenvalues crosses the imaginary axis *leftwards*. These points may represent Hopf bifurcations approached as $\zeta \downarrow \zeta^{***}$ along Γ^+ or Γ^-.

Secondly, and probably more relevant to the present application, it is possible that for $\epsilon > 0$ the branches Γ^+ and Γ^- may not remain stable over all their lengths. Then the two salient eigenvalues (whose zeros respectively determine the critical points ζ^* and ζ_c) are negative for $\zeta^* < \zeta \leqslant \zeta^{**}$ along these branches, coalesce at $\zeta = \zeta^{**}$, become complex conjugates for $\zeta > \zeta^{**}$, and cross the imaginary axis *rightwards* at

$\zeta = \zeta^{***} > \zeta^{**}$. Thus, for $\epsilon > 0$, we still have $\beta = 0$ everywhere along Γ^+ and Γ^-, but these branches may lose stability through a (supercritical) Hopf bifurcation at $\zeta = \zeta^{***}$. For $\epsilon < 0$ in this case, the branches are unstable for all $\zeta > \zeta^*$; complexification occurs as in the first case by coalescence of two positive real eigenvalues, but the complex-conjugate eigenvalues remain to the right of the imaginary axis. In either case the differences $\zeta^{***} - \zeta^*$ and $\zeta^{***} - \zeta^*$ will vanish as ϵ passes through 0.

The main interest of this prototype arises from its implications as a component of a time-dependent model with t-derivative terms entering in a standard fashion, which is exemplified by the class of systems treated in §2.1. Limit cycles breaking the spatial symmetry are known to be a concomitant of the ordering of stationary solutions in a parametric neighbourhood of the double singularity (Guggenheimer 1981). We appear therefore to have identified a qualitative explanation of the observed unsteady motions near the extremities of S_1 and S_3. It is possible that as ζ was raised towards ζ_1 along S_1, for example, a bifurcation into asymmetric steady states was in fact encountered first, and then there was a Hopf bifurcation into a limit cycle centred on one of the asymmetric branches; but we must admit that such progressive departures from symmetry preceding the onset of unsteadiness were not investigated systematically. Asymmetry nevertheless always became conspicuous when the periodic undulations appeared. The great precision that Mullin *et al.* (1987) report to have been needed in their investigation suggests that further experiments made with extraordinary care will be required to settle these remaining aspects of our problem.

The experimental work was done in the laboratory of the Fluid Mechanics Research Institute at the University of Essex during the academic year 1977/78, when S. K. P. was on sabbatical leave from the University of Roorkee. The valuable help given by Mr J. Bartington, Technical Assistant in the laboratory is gratefully acknowledged.

REFERENCES

Balmer, R. T. 1970 The hydrocyst – a stability phenomenon in continuum mechanics. *Nature* **227**, 600–601.

Benjamin, T. B. 1976 Applications of Leray–Schauder degree theory to problems of hydrodynamic stability. *Math. Proc. Camb. Phil. Soc.* **79**, 373–392.

Benjamin, T. B. 1978*a* Bifurcation phenomena in steady flows of a viscous liquid. I. Theory. *Proc. R. Soc. Lond.* A **359**, 1–26.

Benjamin, T. B. 1978*b* Bifurcation phenomena in steady flows of a viscous liquid. II. Experiments. *Proc. R. Soc. Lond.* A **359**, 27–43.

Benjamin, T. B. 1987 Hamiltonian theory for motions of bubbles in an infinite liquid. *J. Fluid Mech.* **181**, 349–379.

Benjamin, T. B. & Mullin, T. 1982 Anomalous modes in the Taylor experiment. *Proc. R. Soc. Lond.* A **377**, 221–249.

Benjamin, T. B. & Olver, P. J. 1982 Hamiltonian structure, symmetries and conservation laws for water waves. *J. Fluid Mech.* **125**, 137–185.

Cliffe, K. A. & Mullin, T. 1985 A numerical and experimental study of anomalous modes in the Taylor experiment. *J. Fluid Mech.* **153**, 243–258.

Debler, W. R. & Yih, C.-S. 1962 Formation of rings in a liquid film attached to the inside of a rotating cylinder. *J. Aerospace Sci.* **29**, 364.

Guckenheimer, J. 1981 On a codimension two bifurcation. In *Proc. Symp. on Dynamical Systems and Turbulence, Univ. of Warwick* 1980. Lecture Notes in Mathematics, vol. 898, pp. 99–142. Springer.

KARWEIT, M. J. & CORRSIN, S. 1975 Observations of cellular patterns in a partly filled, horizontal, rotating cylinder. *Phys. Fluids* **18**, 111–112.

KELLER, J. B., RUBENFELD, L. A. & MOLYNEUX, J. E. 1967 Extremum principles for slow viscous flows with applications to suspensions. *J. Fluid Mech.* **30**, 97–125.

KORTEWEG, D. J. 1883 On a general theorem of the stability of the motion of a viscous fluid. *Phil. Mag.* (5) **16**, 112–118.

LAMB, H. 1932 *Hydrodynamics*, 6th edn. Cambridge University Press. (Dover edition 1945.)

LLOYD, N. G. 1978 *Degree theory*. Cambridge University Press.

MOFFATT, H. K. 1977 Behaviour of a viscous film on the outer surface of a rotating cylinder. *J. Méc.* **16**, 651–673.

MULLIN, T., CLIFFE, K. A. & PFISTER, G. 1987 Unusual time-dependent phenomena in the Taylor–Couette experiment at moderately low Reynolds numbers. *Phys. Rev. Lett.* **58**, 2212–2215.

ORR, F. M. & SCRIVEN, L. E. 1978 Rimming flow: a numerical simulation of steady, viscous, free-surface flow with surface tension. *J. Fluid Mech.* **84**, 145–165.

PHILLIPS, O. M. 1960 Centrifugal waves. *J. Fluid Mech.* **7**, 340–352.

PRITCHARD, W. G. 1986 Instability and chaotic behaviour in a free-surface flow. *J. Fluid Mech.* **165**, 1–60.

RUSCHAK, K. J. & SCRIVEN, L. E. 1976 Rimming flow of liquid in a rotating horizontal cylinder. *J. Fluid Mech.* **76**, 113–125.

SKALAK, R. 1970 Extensions of extremum principles for slow viscous flows. *J. Fluid Mech.* **42**, 527–548.